communications biology

A Nature Portfolio journal

Article

https://doi.org/10.1038/s42003-025-07837-y

Investigating the effect of *Arvcf* reveals an essential role on regulating the mesolimbic dopamine signaling-mediated nicotine reward

Yan Wang[1,6], Zhongli Yang[1,6], Xiaoqiang Shi[1,2], Haijun Han[1], Andria N. Li[3], Bin Zhang[1], Wenji Yuan[1], Yan-Hui Sun[4], Xiao-Ming Li[4], Hong Lian[2,4] ✉ & Ming D. Li[1,5] ✉

The mesolimbic dopamine system is crucial for drug reinforcement and reward learning, leading to addiction. We previously demonstrated that *Arvcf* was associated significantly with nicotine and alcohol addiction through genome-wide association studies. However, the role and mechanisms of *Arvcf* in dopamine-mediated drug reward processes were largely unknown. In this study, we first showed that *Arvcf* mediates nicotine-induced reward behavior by using conditioned place preference (CPP) model on *Arvcf*-knockout (*Arvcf*-KO) animal model. Then, we revealed that *Arvcf* was mainly expressed in VTA dopaminergic neurons whose expression could be upregulated by nicotine treatment. Subsequently, our SnRNA-seq analysis revealed that *Arvcf* was directly involved in dopamine biosynthesis in VTA dopaminergic neurons. Furthermore, we found that *Arvcf*-KO led to a significant reduction in both the dopamine synthesis and release in the nucleus accumbens (NAc) on nicotine stimulation. Specifically, we demonstrated that inhibition of *Arvcf* in VTA dopaminergic neurons decreased dopamine release within VTA-NAc circuit and suppressed nicotine reward-related behavior, while overexpression of *Arvcf* led to the opposite results. Taken together, these findings highlight the role of *Arvcf* in regulating dopamine signaling and reward learning, and its enhancement of dopamine release in the VTA-NAc circuit as a novel mechanism for nicotine reward.

The mesolimbic dopamine projection from the ventral tegmental area (VTA) to the nucleus accumbens (NAc) forms the foundation of nearly all addictive drug-induced reward that motivates continuous drug-seeking behaviors[1–4]. Drugs of abuse have very different mechanisms of action but converge on dopamine reward signaling by producing a series of common functional effects following drug administration[5]. Understanding the underlying molecular and cellular basis of the dopamine reward signaling is crucial for developing more effective treatments for a wide range of addictive disorders.

Arvcf (Armadillo repeat gene deleted in Velo-cardio-facial syndrome) is a p120-catenin family member[6], and some members of this family are known to involve in neuronal development[6,7] and the pathogenesis of various mental disorders such as schizophrenia, autism, and ADHD[8–10]. In our previously reported GWAS study for Chinese smokers, SNP rs148582811 in *ARVCF* was found to be significantly associated with nicotine addiction, which was further replicated in European smoker populations[11,12]. A Mendelian randomization study on alcohol addiction found that *ARVCF* is a causal gene for alcohol addiction[13]. Thus, ARVCF may be a common molecule involved in the regulation of multiple substance addictions, such as nicotine and alcohol addiction. However, the contribution and the underlying mechanism of *Arvcf* 's involvement in drug reward and mesolimbic dopamine signaling are poorly understood.

[1]State Key Laboratory for Diagnosis and Treatment of Infectious Diseases, National Clinical Research Center for Infectious Diseases, National Medical Center for Infectious Diseases, Collaborative Innovation Center for Diagnosis and Treatment of Infectious Diseases, The First Affiliated Hospital, Zhejiang University School of Medicine, Hangzhou, China. [2]Nanhu Brain-computer Interface Institute, Hangzhou, China. [3]Department of Urology, University of Michigan, Ann Arbor, MI, USA. [4]Department of Neurology and Department of Psychiatry of the Second Afiliated Hospital, Zhejiang University School of Medicine, Hangzhou, China. [5]Research Center for Air Pollution and Health, Zhejiang University, Hangzhou, China. [6]These authors contributed equally: Yan Wang, Zhongli Yang.
✉e-mail: honglian@zju.edu.cn; ml2km@zju.edu.cn

The ventral tegmental area (VTA) is rich in cellular diversity, comprising not only various types of glial cells but also a range of neurons, such as dopaminergic, glutamatergic, GABAergic neurons, and combinatorial neurons[14–16]. These cells are known to widely express receptors for addictive substances, such as nicotinic acetylcholine receptors (nAChRs)[2,17,18], opioid receptors[19–22], and cannabinoid receptors[23–25]. Moreover, studies have shown that VTA dopaminergic neuron can be directly activated by addictive drugs[26–28] or indirectly regulated by glutamatergic neurons[29], GABAergic neurons[30,31], and glial cells[32], respectively. At the molecular level, the synthesis, transport, and release of dopamine are precisely regulated by a series of genes[16]. Dysregulation in molecular pathways consisted of these genes can lead to abnormalities in the dopamine signaling and reward-related learning behaviors. Hence, in order to understand the underlying regulatory mechanism of *Arvcf* in dopamine mediated reward learning, it is important to determine how it regulates dopamine release in VTA-NAc circuit at both the molecular and cellular levels.

In this study, by using nicotine reward as a model, we explored the possible role of *Arvcf* in reward learning and dopamine signaling. First, we conducted the CPP behavioral paradigm and in vivo fiber photometry experiments on *Arvcf*-KO mice to determine the role of *Arvcf* in regulating nicotine-induced reward behavior and dopamine release in NAc. Then, we employed RNAscope assay to determine the expression pattern of *Arvcf* in different brain regions and used single nuclei RNA sequencing (SnRNA-seq) technique to determine the expression level of *Arvcf* in various cell types of the VTA. Furthermore, we explored the potential mechanisms by which *Arvcf* affects dopamine release through differential gene expression analysis of SnRNA-seq data, as well as by detecting dopamine-related neurotransmitter concentrations in the VTA. Finally, by generating VTA dopaminergic neuron-specific *Arvcf* knockdown and overexpressing mice, we investigated the regulatory effect of *Arvcf* on dopamine release in the VTA-NAc circuit and nicotine rewarding-related behaviors. Together, this study provided convincing evidence for the role of *Arvcf* in nicotine-induced reward by regulating dopamine synthesis and release.

Results

The genetic deficiency of *Arvcf* reduces the reward behavior and dopamine release level of nicotine stimuli

Before evaluating the role of *Arvcf* in nicotine-induced reward behavior, we conducted an open-field test on both WT and $Arvcf^{-/-}$ mice and found no significant difference in total traveled distance between the WT and $Arvcf^{-/-}$ mice, indicating no obvious motor impairments for $Arvcf^{-/-}$ mice (Fig. 1A; Supplementary Fig. 1A–C). Given that nicotine-induced reward is dose-dependent, a mouse CPP model was employed to determine the role of *Arvcf* involving nicotine reward-related behavior by conditioning on saline or nicotine at the doses of 0.25, 0.5, and 1.0 mg/kg/day (Fig. 1B), respectively. In WT mice, we found that a nicotine dose of 0.5 mg/kg/day resulted in significant place preference for the nicotine-paired chamber whereas the nicotine doses of 0.25 or 1.0 mg/kg/day showed no significant preference for the nicotine-paired side (Fig. 1C, D). In contrast, $Arvcf^{-/-}$ mice showed no obvious preference for three doses of nicotine treatment, indicating that *Arvcf*-KO impaired the nicotine-induced rewarding behavior in mice. Moreover, the statistical analysis of CPP scores stratified by gender for WT and $Arvcf^{-/-}$ mice showed that *Arvcf*-KO led to impaired nicotine reward learning behavior in both male and female mice (Supplementary Fig. 2A, B).

To examine the effect of *Arvcf* on nicotine-induced dopamine release, we employed a genetically encoded DA sensor GRAB (DA2m) to monitor real-time DA release signal in NAc shell during nicotine exposure in WT and $Arvcf^{-/-}$ mice (Fig. 1E, F). Compared with saline control, the dopamine signal in both WT and $Arvcf^{-/-}$ mice increased with nicotine stimulation, but the magnitude of increased signal in WT mice was higher than that of $Arvcf^{-/-}$ mice (Fig. 1G), for example, the average DA2m fluorescence signals increased by 60% in WT mice but only 15% in $Arvcf^{-/-}$ mice (Fig. 1H). Moreover, dopamine signals decayed faster in $Arvcf^{-/-}$ mice, returning to baseline within 0.5 h, but in WT mice it took about 1 h to return to the baseline. After nicotine exposure, the peak and mean value of the signal and the areas under the curve of the two groups all showed a significant decrease in $Arvcf^{-/-}$ mice (Fig. 1I–K). These results indicated that *Arvcf*-KO reduced the nicotine-induced dopamine release level in NAc. Given that the *Arvcf*-KO mice exhibited no nicotine preference and reduced dopamine release in NAc, we conclude that the *Arvcf* deficiency impairs the nicotine reward learning behavior in mice.

Arvcf is highly expressed in VTA dopaminergic neurons and upregulated by nicotine

By using RNAscope technique to assess the spatial distribution of *Arvcf* mRNA in the midbrain region, we found that it was highly expressed in the VTA, less expressed in the cortex and almost no expression in other brain regions (Fig. 2A). To understand the regulatory mechanisms of *Arvcf* for nicotine-induced reward in the VTA, we performed SnRNA-seq analysis on a total of 100,201 single nuclei including 29,120 nuclei from the WT-saline group, 24,794 nuclei from the WT-nicotine group, 23,795 nuclei from the $Arvcf^{-/-}$-saline group, and 22,492 nuclei from the $Arvcf^{-/-}$-nicotine group (Fig. 2B; Supplementary Fig. 3A). Subsequently, UMAP analysis revealed that these single nuclei were assigned into 31 clusters and 11 cell types according to the expression of known gene markers for microglia, endothelial cells, neurons, astrocytes, oligodendrocytes, and oligodendrocyte progenitor cells (Fig. 2C; Supplementary Fig. 3B). Among these 11 cell types, we found that *Arvcf* was mainly expressed in neurons, ependymal cells, and oligodendrocytes progenitor cells (Supplementary Fig. 3C). We further found that the *Arvcf* expression level was increased in the neurons, but not in other cell types, of nicotine-treated WT mice compared to saline-treated WT mice (Supplementary Fig. 3C). Considering that neurons in VTA are primarily responsible for synthesizing and/or releasing various neurotransmitters including dopamine, GABA, and glutamate, all neurons were further subclustered into 17 transcriptionally distinct neuronal subpopulations and were identified as 5 neuronal subtypes based on the expression signature of neuronal markers (Fig. 2D; Supplementary Fig. 4A, B). Further analysis of *Arvcf* expression profiles in neuronal subtypes of saline-treated WT mice revealed that *Arvcf* was expressed across various neuronal subtypes, with the highest expression levels in dopaminergic neurons. Additionally, by comparing the expression levels of *Arvcf* in different types of neurons of nicotine-treated and saline-treated WT mice, it was found that nicotine upregulated the expression of *Arvcf* in the majority of neuronal subtypes (Fig. 2E; Supplementary Fig. 4C).

To confirm enriched *Arvcf* expression in VTA dopaminergic neurons, *Arvcf* mRNA was stained in the VTA with GFP-labeled TH^+ dopaminergic neurons in TH-cre mice infected with AAVs-dio-GFP. As expected, *Arvcf* mRNA were abundant in the VTA (Fig. 2F) with 68% *Arvcf*-positive neurons being dopamine ones whereas 85% dopaminergic neurons were positives for *Arvcf*, indicating that the majority of $Arvcf^+$ cells were co-localized with dopaminergic neurons (Fig. 2G). In addition, a comparison of *Arvcf* mRNA expression in VTA dopaminergic neurons between nicotine- and saline-treated WT mice showed that *Arvcf* expression was significantly increased by nicotine (Supplementary Fig. 5A, B). These findings reveal that *Arvcf* is selectively enriched in VTA dopaminergic neurons and upregulated by nicotine, indicating that *Arvcf* is involved in nicotine-induced neurophysiological changes of VTA dopaminergic neurons.

Reduced TH expression by *Arvcf*-KO leads to decreased dopamine synthesis

Considering the high expression of *Arvcf* in dopaminergic neurons and the key role of dopaminergic neurons in ND, including nicotine-induced reward, we next determined if *Arvcf*-KO impacts gene expression and molecular pathways related to ND in dopaminergic neurons. Differentially expressed genes (DEG) analysis on dopaminergic neurons revealed 368 DEGs between the WT- and $Arvcf^{-/-}$-saline groups, with 229 upregulated genes and 139 downregulated genes (Supplementary Data 1), including those genes associated with ND and dopaminergic functioning, such as *Th*, *kcnj6*, and *gabra2* (Fig. 3A). However, no gene for nAChRs was found to be significantly changed. Further GO analysis of DEGs between the saline-

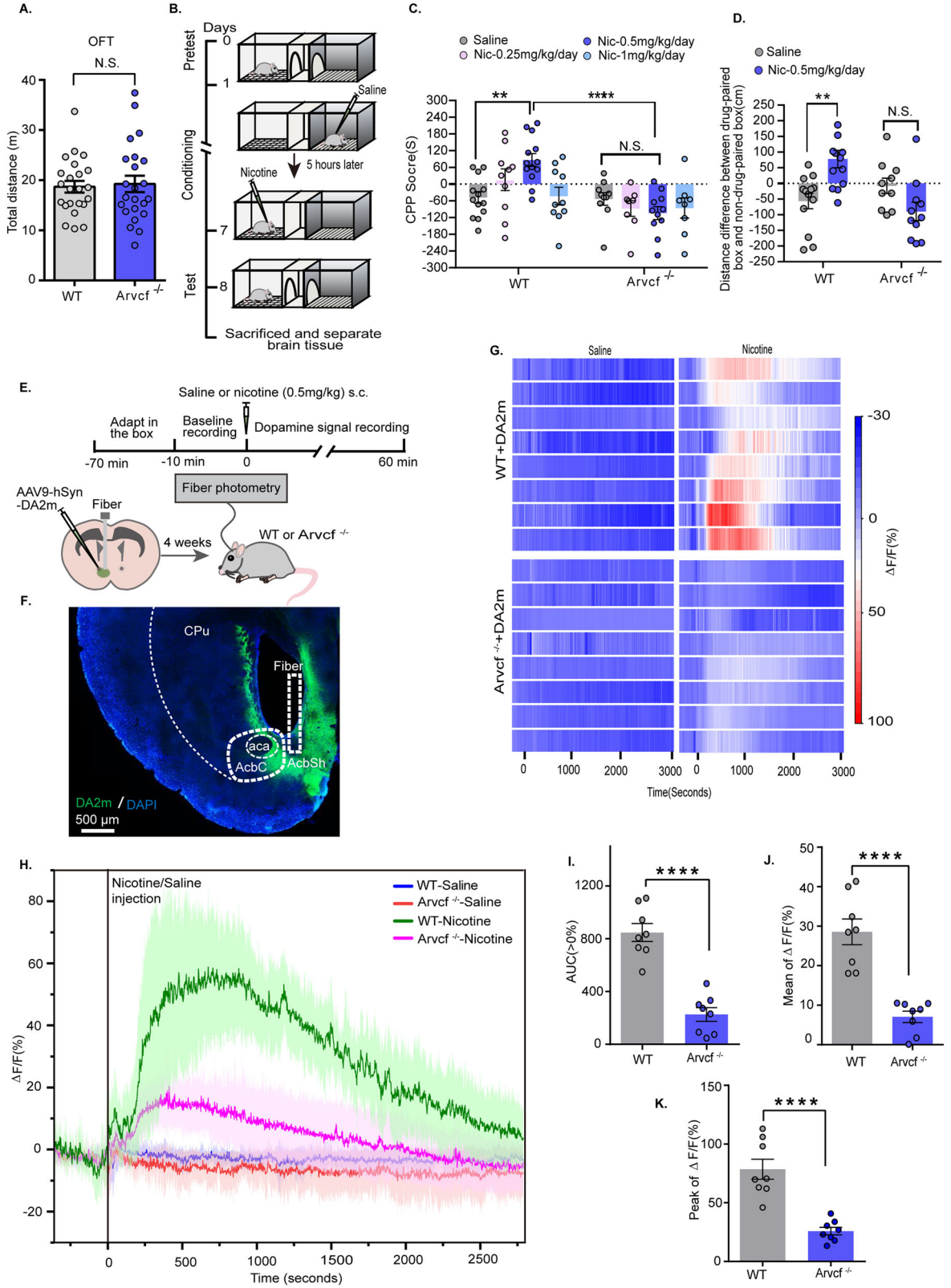

treated *Arvcf*$^{-/-}$ and WT mice revealed that *Arvcf* was mainly involved in the biological processes related to the regulation of dopamine biosynthesis (P_{adj}-value = 0.001, Rich factor =0.25) in dopaminergic neurons in addition to those known pathways associated with neurodevelopment and synaptic morphology (Fig. 3B; Supplementary Data 2)[7,33]. By comparing the DEGs of dopaminergic neurons between the nicotine-treated WT and *Arvcf*$^{-/-}$ mice, 259 upregulated and 49 downregulated genes enriched in the pathways related to postsynaptic density membrane and the development and morphology of neurons were identified (Fig. 3C; Supplementary Data 3 and 4).

Next, we focused on a group of genes known to be important for dopamine biosynthesis including DA synthesis (TH, Ddc and Ar), transportation (Slc18a2, Slc6a3 and Mao-a), and degradation (Comt and

Fig. 1 | The genetic deficiency of *Arvcf* reduces the reward learning behavior and dopamine release level of nicotine stimulation. **A** Quantification of total moving distance during a 15 min OFT for naive WT and *Arvcf*$^{-/-}$ mice. $n = 23–24$ mice/group and unpaired Student's *t*-test was used in comparisons. **B** Schematic protocol of CPP for evaluating nicotine-inducted rewarding behavior in WT and *Arvcf*$^{-/-}$ mice. **C** CPP scores of WT and *Arvcf*$^{-/-}$ mice in test phase. **D** Comparison of the travel distance between WT and *Arvcf*$^{-/-}$ mice on the paired box of saline and nicotine (0.5 mg/kg) in test phase. For (**C**, **D**), $n = 8–13$ mice/group and two-way ANOVA followed by Bonferroni's multiple comparison test was used in comparisons. **E** Schematic of recording system for obtaining dopamine release signals with fiber photometry under saline or 0.5 mg/kg dose of nicotine stimulation. **F** Representative images of DA2m sensors virus infection and fiber implantation in NAc. Scale bar, 500 μm. **G**, **H** Effect of *Arvcf* on dopamine release in NAc in response to nicotine. Heatmap (**G**) and average (**H**, mean ± 95% CI; vertical line, start of nicotine or saline injection) dopamine transients of neurons in NAc of WT mice ($n = 8$) and *Arvcf*$^{-/-}$ mice ($n = 8$) under nicotine or saline stimulus. Statistics for the area under the curves (**I**), mean values (**J**) and peak values (**K**) of the transients of dopamine signal between WT mice and *Arvcf*$^{-/-}$ mice under nicotine stimulation; unpaired Student's t-test was used in comparisons. Data are presented as Mean± S.E.M.; $^{*}p < 0.05$, $^{**}p < 0.01$,$^{***}p < 0.001$, $^{****}p < 0.0001$, N.S., not significant.

Aldh1a1). Our SnRNA-seq results showed that TH expression in dopaminergic neurons was significantly decreased in both saline- and nicotine-treated *Arvcf*$^{-/-}$ mice relative to the WT mice with or without nicotine treatment, but no obvious change was found in the expression of other selected genes (Fig. 3D; Supplementary Fig. 6A). Meanwhile, immunofluorescent staining for TH in the VTA of WT and *Arvcf*$^{-/-}$ mice produced consistent results at the protein level, i.e., both the mean fluorescence intensity and the number of TH^{+} cells were significantly lower in *Arvcf*$^{-/-}$ mice (Fig. 3E–G). Further examination of dopamine concentration by LC-MS analysis of VTA tissues from the WT and *Arvcf*$^{-/-}$ mice showed that the dopamine concentration and one of its metabolites, homovanillic acid (HAV) in the VTA of *Arvcf*$^{-/-}$ mice was significantly decreased compared with that of WT mice (Fig. 3H–K). Together, these results indicate that the loss of *Arvcf* downregulates the expression of TH and dopamine synthesis, which may underlie the impairment of nicotine-induced reward behavior and reduction of dopamine release level in NAc of *Arvcf*$^{-/-}$ mice.

VTA dopaminergic *Arvcf* can mediate nicotine-induced rewarding effect and TH expression

To characterize the precise role of *Arvcf* in dopaminergic neurons, *Arvcf* was selectively knocked down (*Arvcf*-KD) or overexpressed (*Arvcf*-OE) in VTA dopaminergic neurons by microinjection of AAVs expressing Cre-inducible sh*Arvcf* or *Arvcf* into the VTA of TH-Cre mice (Fig. 4A), and the knockdown or overexpression efficiency of *Arvcf* mRNA in VTA dopaminergic neurons were verified by RNAscope analysis (Supplementary Fig. 7A–D). Further immunofluorescent staining against TH showed that the *Arvcf*-KD in dopaminergic neurons led to a significant decrease in the mean expression of TH (Fig. 4B, C), while *Arvcf*-OE led to an opposite result (Fig. 4D, E). These findings imply that *Arvcf* in dopaminergic neurons regulates dopamine synthesis through TH expression.

Compared with the corresponding control group, the open field test results revealed no significant changes in the total traveled distance between the *Arvcf*-KD and *Arvcf*-OE mice, suggesting that the change in the expression level of *Arvcf* in the VTA dopaminergic neurons has no obvious effect on the motor ability of mice (Fig. 4F, G). We next examined the changes of nicotine-induced reward behavior after the VTA dopaminergic *Arvcf* expression was altered. By using a nicotine dose of 0.5 mg/kg/day for CPP paradigm on both *Arvcf*-KD and *Arvcf*-OE mice, we found that *Arvcf*-KD in VTA dopaminergic neurons led to significantly decreased preference score and shorter moving distance in mice for nicotine-paired chamber compared with nicotine-treated mice with normal *Arvcf* expression, which was consistent with the result of *Arvcf*$^{-/-}$ mice (Fig. 4H, I). However, *Arvcf*-OE in VTA TH^{+} cells resulted in significantly increased preference scores and longer moving distances of mice for nicotine-paired chamber compared with the controls (Fig. 4J, K). These results demonstrate that *Arvcf* expression in dopaminergic neurons has an important role in regulating the rewarding effect of nicotine in mice.

Specifically altering *Arvcf* expression in dopaminergic neurons affects dopamine transmission in the VTA-NAc circuit

Given dopamine transmission in VTA-NAc circuit is critical for mediating both drug-rewarding and natural-rewarding behaviors, we then determined whether *Arvcf* in VTA dopaminergic neurons could mediate the nicotine-induced dopamine projection in the VTA-NAc circuit. The fiber photometry results of DA2m signal showed that the degree of NAc dopamine increase in the *Arvcf*-KD group was obviously lower than that in the control group by nicotine stimulation (Fig. 5A, B), and the results of peak value and AUC of dopamine signal in the *Arvcf*-KD group were significantly reduced (Fig. 5C, D). Conversely, *Arvcf*-OE markedly facilitated circuit dopamine transmission (Fig. 5E, F), as evidenced by the significantly increased peak value (Fig. 5G) and AUC (Fig. 5H) of the dopamine release level compared with the control group in response to nicotine treatment.

We further examined the role of VTA dopaminergic *Arvcf* in regulating dopamine release induced by natural reward stimuli such as food intake, drinking and social investigation. The NAc dopamine signal transiently increased in the testing male mice of both *Arvcf*-KD and control groups during the initial social investigation with male or female introducers from different home cages. However, we observed that the peak value of dopamine signal changes in *Arvcf*-KD male mice were significantly lower during both male and female social investigations compared to the control group mice (Fig. 5I, J). Following the food and water stimuli, the dopamine released signal in NAc of *Arvcf*-KD male mice were also lower than that in the control group (Fig. 5K, L). These findings suggested that *Arvcf* in dopamineric neurons can regulate both nicotine-reward and natural-reward induced dopamine release in the VTA-NAc circuit, implying that *Arvcf* may play an important role in regulating widely reward-related processes.

Discussion

In this study, we demonstrate that *Arvcf* plays an important role in the development of nicotine reward by using both nicotine CPP paradigm and fiber photometry. RNAscope and SnRNA-seq analysis revealed that *Arvcf* is specifically expressed in VTA dopaminergic neurons and up-regulated by nicotine. Our mechanistic studies further revealed that *Arvcf* promotes dopamine synthesis by enhancing the expression of TH in VTA dopaminergic neurons and thus led to the dysfunction of nicotine-induced dopamine release in the NAc and the impairment of reward-related behaviors in mice.

The rewarding effect of nicotine is one of the main drivers to keep smoking[2,34–36]. The mesolimbic dopamine projection originating from the VTA to NAc controls almost all reward processing including drug and natural reward stimuli[37], and increased dopamine release in the NAc is known to play an important role in mediating reward-seeking behaviors[2,38–42]. By employing the commonly used CPP model to assess the rewarding effects of addictive drugs[43,44], we found that *Arvcf*-KO mice had an impaired nicotine-induced reward behavior. By combining the genetically-encoded GPCR-Activation-Based-DA sensors[45] with the fiber-optic recording system, we successfully detected dopamine release in NAc of freely-behaving mice in real-time and found that the role of *Arvcf*-KO led to a significant reduction in DA release in response to nicotine reward stimuli. These findings strongly indicate that the positive regulating role of *Arvcf* on nicotine-induced dopamine release and reward learning behavior.

By using the novel and powerful RNAscope analysis technique, we found that *Arvcf* was abundantly expressed in the VTA region, a key structure of the mesolimbic dopamine system. The cellular heterogeneity of VTA leads to the complexity of the mechanisms by which it affects drug reward[14,46]. By comparing snRNA-seq data from the VTA region of nicotine- and saline-treatment WT mice, we found that the expression of

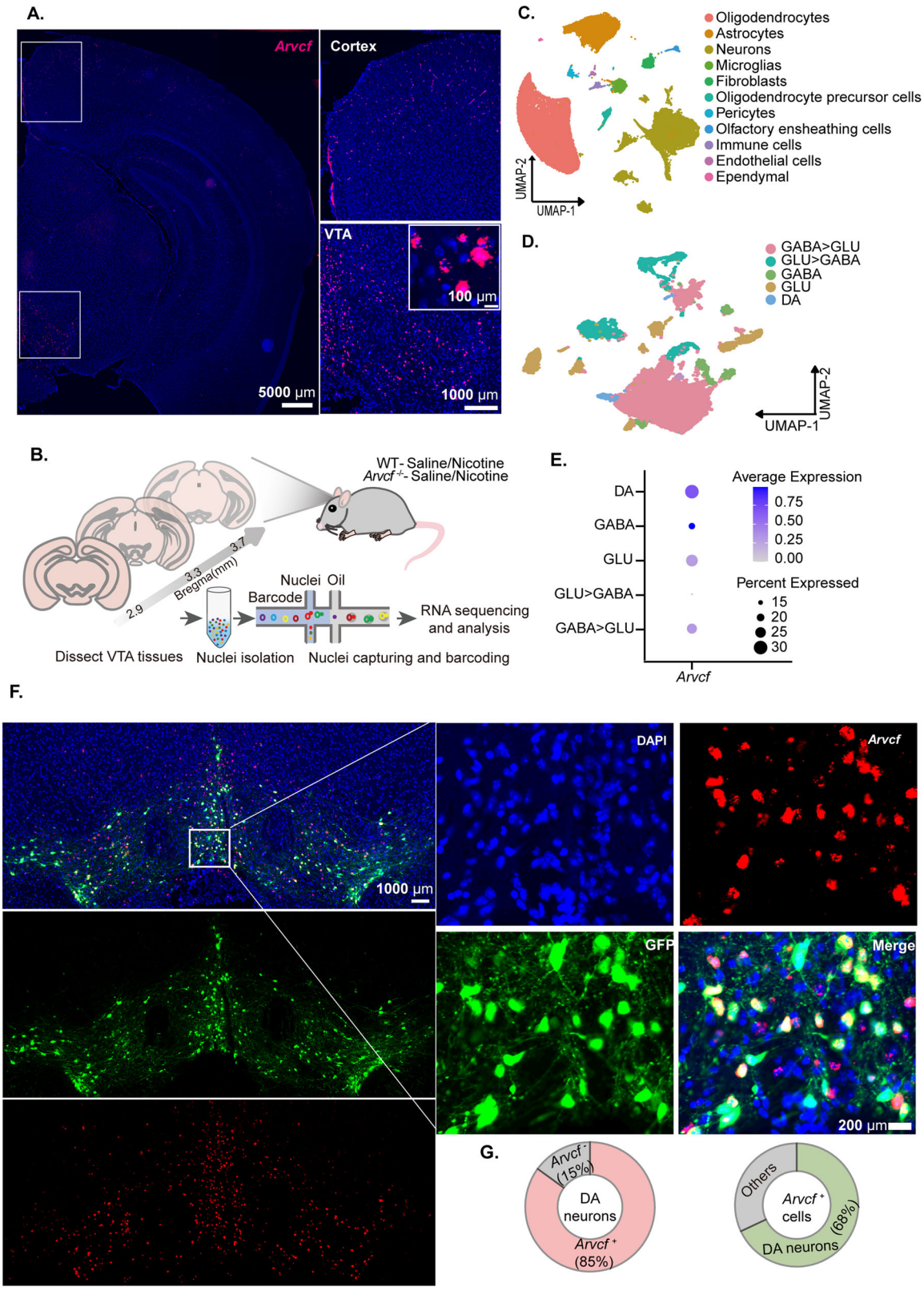

Arvcf appeared to be cell-specific, with a high expression in neurons, ependymal cells, and oligodendrocyte precursor cells, but almost no expression in glial cells. Considering the critical role of neurons in nicotine reward, in this study, we then specifically focused on the function of *Arvcf* in neurons. We found that *Arvcf* is highly expressed in dopaminergic neurons and upregulated by nicotine, which was further validated by the localization analysis of *Arvcf* 's mRNA in TH^+ dopaminergic neurons. Our finding of such a region- and neuron-specific expression pattern of *Arvcf* might explain the results from other ScRNA-seq analysis studies where *Arvcf* was not found to be significantly enriched in the neurons of the primary visual cortical region in mice[6,47]. However, there is no doubt that further exploring the expression and role

Fig. 2 | *Arvcf* is highly expressed in VTA dopaminergic neurons. A Representative image of *Arvcf*'s mRNA (red) localization in naive WT-C57BL/6 J mice coronal brain slice (left, n = 3 male mice), scale bar = 5000 μm; mRNA of *Arvcf* (red) at cortex (right, upper) and VTA (right, lower), scale bar = 1000 um, magnified scale bar, 100 μm. **B** Experimental design of snRNA-seq. 10×Genomics experimental workflow was applied to nuclei isolation from VTA tissues of 12 male mice in 4 experimental groups (WT-saline, WT-nicotine, $Arvcf^{-/-}$-saline, $Arvcf^{-/-}$-nicotine, n = 3/group). **C** Uniform approximation and projection (UMAP) plot of 100,201 nuclei from 12 mice VTA samples with the 11 color-coded cell types based on the expression pattern of canonical marker genes. **D** UMAP plot of neuronal subclusters for identified 26,790 neurons and annotations for the neuronal subclusters with color-coded neuron types based on the expression of markers corresponding to each neurotransmitter system. GABA = GABAergic neurons; GLU = Glutamatergic neurons; DA = Dopaminergic neurons; GABA > GLU and GLU > GABA defined as combinatorial neurons capable of conbinatorial neurotransmitter release. **E** Feature plot of expression values for *Arvcf* of 6 identified neuronal cell types from 3 WT-saline group mice. **F** *Arvcf* mRNA (red) and GFP (green) co-staining representative image of WT mice (n = 3 mice). Arrows, colocalization of *Arvcf* and GFP-labled TH^+ dopaminergic neurons. Scale bar, 1000 μm. Magnified scale bar, 200 μm. **G** Proportion of *Arvcf*-positive cells in dopaminergic neurons (left) and of dopaminergic neurons in *Arvcf*-positive cells (right: 3 slides from 3 mice).

of *Arvcf* in ependymal cells and oligodendrocyte precursor cells in the future may help us to better understand the biological function of *Arvcf*.

By performing the DEGs and pathway enrichment analysis of SnRNA-seq data in dopaminergic neurons between *Arvcf*-KO and WT mice, we found that many genes involved in neuronal development, synaptic morphology, and dopamine biosynthesis were significantly changed. From our analysis of the genes related to dopamine synthesis based on its crucial role for maintaining dopamine homeostasis, we found that the expression of TH, a limited enzyme for dopamine synthesis, was significantly down-regulated by *Arvcf*-KO, but the expression of dopamine metabolism- and transport-related genes did not changed significantly. Furthermore, selectively over-expressing *Arvcf* in dopaminergic neurons significantly increased the expression of TH, while selectively knockdown *Arvcf* led to a decreased expression of TH. Subsequently LC/MS analysis of dopamine concentration in VTA revealed that *Arvcf*-KO led to a significantly decreased dopamine concentration in the VTA compared to WT mice. Taken together, we concluded that VTA dopaminergic *Arvcf* enhanced dopamine synthesis by up-regulating the expression of TH. This newly identified role of *Arvcf* for its involvement in dopamine synthesis suggest that *Arvcf* may likely serve as an indispensable regulatory molecule of dopamine release, which is vital to the development of nicotine reward.

Herein, by specifically altering the expression level of *Arvcf* in the VTA dopaminergic neurons of TH-Cre mice and using an optical fiber recording system, we detected the dopamine release levels of NAc under nicotine stimuli in these mice and found that overexpression of VTA dopaminergic *Arvcf* led to an increased dopamine release in NAc of mice in response to nicotine reward stimuli. Conversely, knocking down *Arvcf* expression in these neurons led to a decreased dopamine release in NAc in response to nicotine stimuli. Consequently, the CPP paradigm revealed that the function of *Arvcf* in dopaminergic neurons directly facilitated the nicotine reward behavior in mice. Together, these results demonstrate that *Arvcf* in VTA dopaminergic neurons is a critical contributor to dopamine release in the VTA-NAc circuit and nicotine reward, which may form the foundation for precise targeting treatment of nicotine addiction if the expression level of *Arvcf* in VTA dopaminergic neurons can be validated in smokers in future work.

Some inevitable methodological limitations of the current study warrant further comment. Firstly, human nicotine dependence is a complex process that encompasses a variety of behavioral patterns, including smoking initiation, nicotine dependence, withdrawal, and relapse[48,49]. The CPP paradigm has high validity in modeling nicotine reward, and craving induced by nicotine cues in humans[50]. But the non-contingent, passive subcutaneous injection of nicotine in this paradigm is known to be different from tobacco smokers[51]. Here, we have demonstrated the promoting role of *Arvcf* in nicotine reward using the CPP paradigm, but it is necessary to improve the administration method of the CPP model to make it more similar to the manner of human smoking in the future. Furthermore, using nicotine self-administration and withdrawal models to explore the effects of *Arvcf* on nicotine withdrawal and relapse behaviors in future will contribute to a comprehensive understanding of the role of *Arvcf* in nicotine dependence. Secondly, it is known that the mesolimbic dopamine system also plays a complex and pivotal role in the initiation, regulation, and learning of movement, particularly the dopaminergic neurons in the substantia nigra pars compacta adjacent to VTA[52,53]. In this study, by using *Arvcf*-KO mice and conditional VTA dopaminergic *Arvcf* knockdown and overexpression mice, we confirmed that the expression of *Arvcf* promotes the synthesis and release of dopamine, further suggesting the potential regulatory role of *Arvcf* in dopamine-mediated motor behavior. Although our open-field test results from these mice showed that the alteration of the expression of *Arvcf* had no significant effect on the spontaneous motor activity of mice, future analysis of the regulatory role of *Arvcf* in motor coordination and intensity using gait analysis systems and rotarod tests will be critical for understanding the role of *Arvcf* in motor-related diseases mediated by dopamine dysregulation, such as Parkinson's disease.

The protein encoded by the XRCC5 gene is the 80-kilodalton subunit of the Ku heterodimer protein, also known as ATP-dependent DNA helicase II or DNA repair protein XRCC5[54]. It primarily involves in the repair of DNA double-strand breaks[54] and it also has been reported to function as a negative transcription regulator to inhibit the transcription of downstream genes[55], such as STK4[56], CLC-3[57],and COX-2[58]. In our previous study, we discovered that XRCC5 binds to the SNP rs148582811, regulating ARVCF expression in an allele-specific manner[11]. The SNP rs148582811 located in the enhancer region of the ARVCF gene has a higher frequency of the T allele in the smokers, while in the non-smokers, this SNP mainly exists in the form of the C allele. Compared to the C allele, when the rs148582811 exists as the T allele, the binding of XRCC5 to the region where rs148582811 is located significantly decreases, while the expression of ARVCF significantly increased. In the current study, we observed that *Arvcf* expression was upregulated in VTA brain region of mice following nicotine treatment, and the aforementioned regulatory mechanism provides an explanation for the nicotine-induced upregulation of *Arvcf* expression. More importantly, we have discovered that *Arvcf* is essential for nicotine reward and promotes it by increasing TH expression and dopamine levels. It has been reported that ARVCF interacts with N-cadherin, and that abnormal cleavage of N-cadherin can lead to a reduction in TH expression[59]. Whether ARVCF regulates the expression of TH by interacting with N-cadherin and affecting the cleavage of N-cadherin warrants further investigation. It has long been recognized that VTA dopamine can also project to other target areas, such as the prefrontal cortex, amygdala, and hippocampus to modulate the processing of emotions, memory, and cognition[60–63], we now offer a working hypothesis for the involvement of *Arvcf* in dopamine signaling mediated disorders, such as addiction, depression, and parkinson's disease through theXRCC5-*Arvcf*-N-cadherin signal pathway (Fig. 6).

In sum, this study demonstrates a promoting role of VTA dopaminergic *Arvcf* in regulating dopamine synthesis and release in VTA-NAc circuit, suggesting a new cellular and molecular mechanism for the involvement of *Arvcf* in nicotine reward and other dopamine-mediated rewarding associated psychiatric disorders.

Methods

Animals

Wild-type C57BL/6 J and transgenic mice including $Arvcf^{-/-}$ (Strain No. T010888) and TH-Cre (Strain No. 008601) mice were obtained from the Gempharmatech Company (Jiangsu, China) or the Jackson Laboratory (Shanghai, China). $Arvcf^{-/-}$ mice were generated on a C57BL/6 J background via the CRISPR/Cas9 system. $Arvcf^{+/-}$ mice were bred to produce $Arvcf^{-/-}$ mice and their littermate WT controls. All transgenic mice and their littermate WT controls were determined by genotyping. All mice used in the

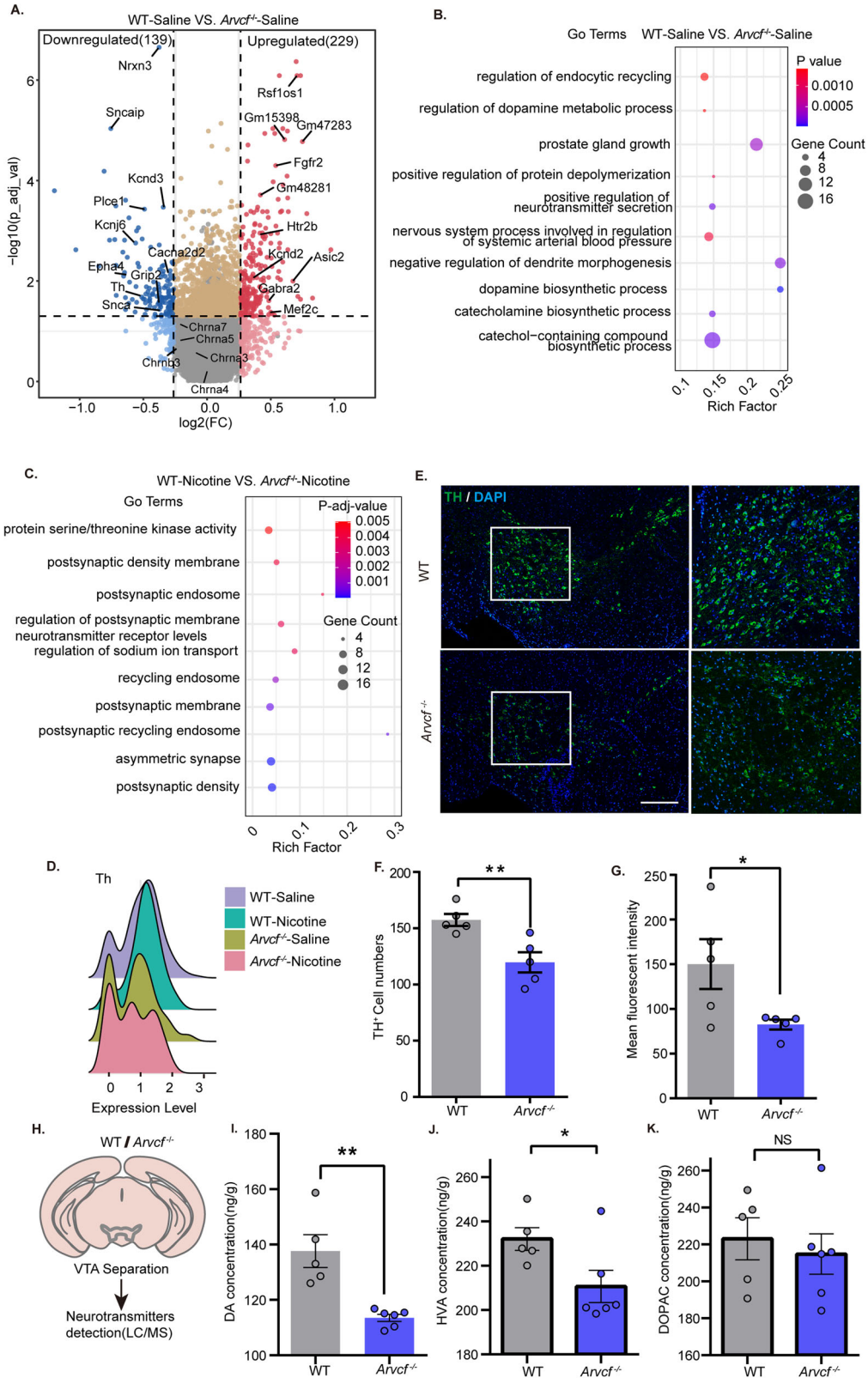

study were 6-to-14 weeks old and were group-housed under a 12 h light-dark cycle with food and water ad libitum unless specified. Behavioral tests were performed on 8-to-10-week-old mice, and their age at the time of conducintg SnRNA-seq analysis was 10-to-12-week-old. Six-to-seven-week-old mice were used for the virus injection experiments, and their age at the time of fiber photometry was 11-to-12-week old. Slices for RNAscope and immunofluorescence staining are generally prepared in mice around 12 weeks of age. In all behavioral and in vivo dopamine recording experiments, the gender distribution in each group was approximately equal. All mice were randomly assigned to groups and were naive to all behavioral tests at the start of each experiment. All experiments were approved by the Animal Care and Use Committee at Zhejiang University and conducted in

Fig. 3 | Reduced TH expression by *Arvcf* deletion leads to decreased dopamine biosynthesis. A Volcano plot showing differential expression genes (DEGs) of dopaminergic neurons between WT and $Arvcf^{-/-}$ mice. Genes labeled in blue are downregulated in $Arvcf^{-/-}$ mice compared to WT mice, while genes labeled in red are upregulated in $Arvcf^{-/-}$ mice. **B**, **C** Gene Ontology (GO) biological pathway enrichment dot plot of top 20 pathways enriched significantly for DEGs of dopaminergic neurons in $Arvcf^{-/-}$ vs. WT mice with saline-control (**B**) or $Arvcf^{-/-}$ vs. WT mice with nicotine-treatment (**C**). **D** Ridge diagram of expression level forTh of dopaminergic neurons in WT and $Arvcf^{-/-}$ mice treated with saline or nicotine. **E** Representative images of immunofluorescent staining of TH (green) in VTA of WT mice (5 brain slices from 5 mice) and $Arvcf^{-/-}$ mice (5 brain slices from 5 mice). Scale bar, 300 μm. **F**, **G** Statistics for number of TH^+ cells (**F**) and mean fluorescent intensity of TH (**G**) between WT mice and $Arvcf^{-/-}$ mice. **H** Schematics of LC/MS detection for the concentration of VTA neurotransmitter in WT and $Arvcf^{-/-}$ mice. **I**–**K** Statistics of the concentration of dopamine (**I**) and dopamine metabolisms HAV (**J**) and DOPAC (**K**) between WT ($n = 5$ male mice) and $Arvcf^{-/-}$ mice ($n = 6$ male mice). Data are presented as Mean ± S.E.M.; two-sided unpaired t-test, $^*p < 0.05$, $^{**}p < 0.01$. N.S. = Not significant, $p > 0.05$.

accordance with the National Institutes of Health Guidelines for the Care and Use of Laboratory Animals (Approval No. 2023-596).

Open field test (OFT)

Mice were individually placed in the central zone of an open field (45 × 45 × 45 cm) chamber for 15 min. Their paths were recorded by using video camera and analyzed with Any-maze software (v.6.0, Stoelting). Locomotor activity was evaluated based on the total distance traveled within 15 min.

Conditioned place preference (CPP) test

The CPP test was conducted in an apparatus consisting of two chambers (50 × 25 × 30 cm) with completely different contexts (RWD, Shenzhen, China). One chamber had white walls with a grid floor and the other had dark walls with a floor containing holes. The intermediate box (20 × 15 × 30 cm) separates the chambers at both ends with removable channels that could isolate the mice within the chambers or allow them to move freely between the two chambers. In the pre-test phase, mice were allowed to move freely within the apparatus for 15 min to determine the mice's natural preference for chamber context. The less preferred chamber served as the drug-paired side, while the opposite chamber was defined as the saline-paired side. During the one-week conditioning phase, mice were then confined to the saline-paired side chamber for 30 min after subcutaneous injection of saline and mice were subsequently confined to the nicotine paired side for 30 min following nicotine subcutaneous injection (0.25, 0.5, and 1.0 mg/kg per injection, with a pH of 7.0, expressed as the free base of nicotine sulfate; Sigma-Aldrich) after a 5-h resting. On the testing phase, mice were allowed to move freely in two chambers again for 15 min in a drug-free state and the activity trace of mice was recorded with an overhead camera. Locomotor distance and duration within the CPP apparatus were automatically analyzed using Any-maze software. The preference score was calculated as the difference in time spent on the drug-paired side versus the saline-paired side[64].

Viruses

The virus AAV9-hsyn-DA2m (titer: 4.26×10^{12} Vg/ml) was used to detect dopamine release signal in NAc brain region of mice, which was purchased from the WZ Bioscience (Shandong, China). For *Arvcf* conditional knockdown, the following short-hairpin sequence was used: 5′-GCTTTGAGAACGAGGGTATTA-3′. The high titers of engineered AAV (AAV9-DIO-GFP-shmir*Arvcf*, 9.3×10^{12} Vg/mL) and compared negative control (AAV9-DIO-GFP-shmirRNA, 5.7×10^{12} Vg/ml) were produced by OBiO Technology (Shanghai, China). For *Arvcf* conditional overexpression, the high titer of engineered AAV (AAV9-DIO-GFP-*Arvcf*, 4.28×10^{12} Vg/mL) and compared negative control (AAV9-DIO-GFP, 2.77×10^{12} Vg/mL) were all purchased from OBiO Technology (Shanghai, China).

Stereotaxic injection and optical fiber implant

Mice were anesthetized with sodium pentobarbital (50 mg/kg, *i.p.* injection) and immobilized in a stereotaxic apparatus (RWD, Shenzhen, China) for virus injection. After dissecting the skin and locating the target brain region using a 10 μL glass microsyringe with a 10–15 μm diameter tip (Hamilton, Nevada, USA), the skull above the target brain area was drilled with a dental drill, and the skull debris was carefully removed. Syringe pumps (KD Scientific, 78-8130, USA) were used to inject the virus with a controlled injection speed and volume. For photometric recording of dopamine release signal in the NAc, 200 nL of AAV9-hsyn-DA2m were injected into the NAc shell (AP: +1.6 mm; ML: +0.85 mm; DV: −4.4 mm; relative to bregma) at a speed of 50 nL/min. The injection needle was slowly withdrawn 10 min after the last injection. Four weeks after viral injection, a mono fiber-optic cannula (200 μm in diameter, N.A. = 0.37, 5 mm; Inper Inc., Hangzhou, China) was then implanted through the same route of viral injection to above the NAc shell (AP: +1.6 mm; ML: +0.85 mm; DV: −4.2 mm) and mounted on the skull using screws and dental cement. Following each surgery, mice were allowed to recover from anaesthesia on a heat pad.

The coordinates of VTA injection were as follows: AP, −3.2 mm; ML, ±0.35 mm; DV, −4.6 mm (relative to bregma). To conditionally overexpress or knock down *Arvcf* in VTA TH^+ neurons, TH-Cre mice were bilaterally injected with 150 nL AAV9-DIO-GFP-*Arvcf* or AAV9-DIO-GFP-shmir*Arvcf* at a speed of 30 nL/min. Regarding behavioral assessments, mice were allowed to recover for four weeks following the viral injection prior to initiate each experiment. For in vivo fiber photometry, TH-Cre mice were simultaneously injected with AAV9-hsyn-DA2m in the NAc. Four weeks post-viral injection, the fiber-optic cannula was implanted and mice were allowed to have 7 days for recovery after cannula implantation.

Fiber photometry assessment of nicotine-induced dopamine release

One week after fiber-optic cannula implantation, dopamine fluorescence signals were recorded by using a fiber photometry apparatus (Inper, China). Mice were allowed to acclimatize in a transparent chamber (70 × 70 × 50 cm) for 1 h before recording. The implanted fiber and commutator were connected via a 2-meter-long optical fiber and the 470 nm and 410 nm light sources were given alternately, with 410 nm being used as the internal control to correct motion signal interference. To simultaneously capture and align mouse behavior and fluorescence signals in the same screen recording, the camera was positioned above the chamber to track each mouse. The Inper Studio software (v.0.5.4, Inper Inc) was used for parameter setting and signal collection. After the fluorescence signal stabilized, the baseline signal was recorded for 10 min. Then mice were injected with saline subcutaneously and the signal was recorded for 1 h. With the same procedure and parameters, the mice were also recorded for fluorescence intensities stimulated by 0.5 mg/kg nicotine until the signal returned to baseline. Finally, we used Inper Data Process (v. 0.7.2, Inper) software to analyze photometric data and calculated ΔF/F0 using a baseline 300 s before the start of nicotine stimulation. The real-time dopamine signals were analyzed using the Origin 8 software.

Preparation of VTA nuclei suspensions and libraries for SnRNA-seq analysis

Twelve WT and $Arvcf^{-/-}$ male mice from saline and nicotine-treated group (0.5 mg/kg/day) of CPP test (3 animals per group) were used for SnRNA-seq analysis of VTA region. On the day by the completion of CPP testing, we performed nicotine/saline injections and subsequent VTA brain tissue dissection on four groups of mice (three per group) in a batch-wise manner. The brain tissues of each mouse group were rapidly isolated within 2 hours after a subcutaneous injection of nicotine (0.5 mg/kg) or saline. Brain tissue was washed three times with cold PBS to remove residual surface blood. The container of vibratome (VT1200s, Leica) was filled with ice-cooled PBS, and the brain tissue was sectioned into 300-μm-thick coronal slices. The coronal

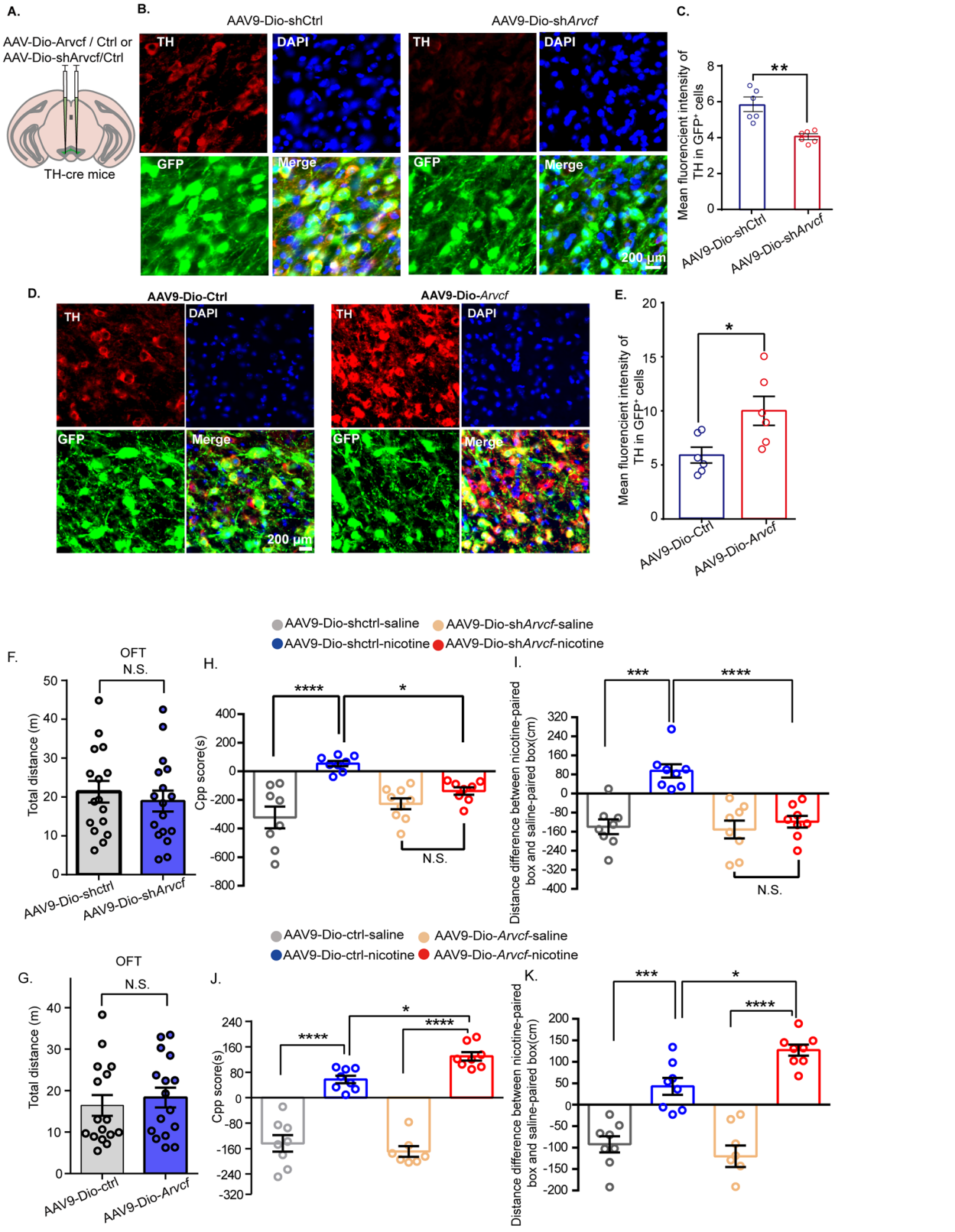

brain slices with bregma between −2.9 and −3.7 mm were collected to isolate VTA tissue under a dissection microscope (Ivesta 3, Leica), snap-frozen in liquid nitrogen, and stored at −80 °C.

The frozen tissue was chopped into 1–2 mm^2 pieces and homogenized in 2 mL of ice-cold Nuclei EZ Lysis buffer (Sigma-Aldrich, NUC-101, USA) supplemented with protease inhibitor (Roche, 5892791001, Switzerland) and RNase inhibitor (Promega, N2615, USA). Homogenates were incubated on ice for 5 min, and an equal volume of ice-cold 4% bovine serum albumin (BSA, Sigma, USA) was added for stopping lysis. The supernatant was then centrifuged at 300 × *g* for 10 min at 4 °C and was resuspended with 4 mL lysis buffer. Cell debris and large clumps were removed using 20 μm filters. To further remove debris, Myelin Removal Beads II (Miltenyi Biotec,

Fig. 4 | VTA dopaminergic *Arvcf* can mediate nicotine-induced rewarding behavior and TH expression. A Schematic of injection of *Arvcf* knockdown or overexpressed virus to VTA dopaminergic neurons on TH-cre mice. **B** Representative images of the expression of TH (red) in GFP^+ *Arvcf* knockdown neurons and the corresponding control neurons at VTA; scale bar, 200 μm. **C** Statistical parameters of the mean fluorescence intensity in *Arvcf* selectively knockdown group (6 slices from 3 male mice) and the corresponding control group (6 slices from 3 male mice). Two-tailed unpaired t-tests, $^{**}p < 0.01$. **D** Representative images of the expression of TH (red) in GFP^+ *Arvcf* overexpression neurons and the corresponding control neurons at VTA; scale bar, 200 μm. **E** Statistics of the mean fluorescence intensity in *Arvcf* selectively overexpression group (6 slides from 3 male mice) and the corresponding control group (6 slides from 3 male mice). Two-tailed unpaired t-tests, $^{**}p < 0.01$. **F**, **G** Total traveled distance of *Arvcf* selectively knockdown group (**F**) and overexpression group (**G**) and their corresponding control groups of mice in OFT. n = 16-17 mice/group. **H**, **I** Detection of nicotine rewarding behavior after selectively knockdown *Arvcf* in dopaminergic neurons of mice. Comparison of CPP scores (**H**) and travel distance (**I**) between AAV-Dio-shCtrl group mice and AAV-Dio-sh*Arvcf* group mice conditioned with 0.5 mg/kg nicotine or saline. $n = 8–9$ mice/group; data were analyzed by two-way ANOVA followed by Bonferroni's multiple comparison test. **J**, **K** Detection of nicotine rewarding behavior after selectively overexpressing *Arvcf* in dopaminergic neurons of mice. Comparison of CPP scores (**J**) and travel distance (**K**) between AAV-Dio-Ctrl group mice and AAV-Dio-*Arvcf* group mice conditioned with 0.5 mg/kg nicotine or saline. $n = 7–8$ mice/group. Data were analyzed by two-way ANOVA followed by Bonferroni's multiple comparison test. Data are shown as Mean ± S.E.M.; $^{*}p < 0.05$, $^{**}p < 0.01$,$^{***}p < 0.001$, $^{****}p < 0.0001$, N.S., not significant.

Germany) were applied according to the manufacturer's instructions. Nuclei were washed 1–2 times and resuspended in buffer containing PBS, 1% BSA, and RNase inhibitor, then collected by centrifugation at 300 × *g* for 5 min at 4 °C. The nuclei were stained by DAPI (Thermo Fisher, USA) and counted manually under a fluorescent microscope (BX53, Olympus). The nuclear suspension was diluted to a concentration of 700–1200 cells/μL prior to loading into the 10× Chromium instrument. Chromium™ Single Cell 3' Reagent Kit v3.1 (10X Genomics PN-100121 and PN-100128) was used for library preparation which include nuclear barcoding, cDNA amplification, and library construction according to the manufacturer's user guides. Libraries were sequenced on the Illumina NovaSeq 6000 System at LC-Bio Technology Co., Ltd. (Hangzhou, China).

SnRNA-seq data processing

The raw sequencing data were processed by the Cell Ranger (v3.1.0), which performed sequencing read alignment, gene expression quantification, and integration of cells from different samples using the mouse genome reference GRCm38/mm10. The DoubletFinder function of Seurat package was used to filter out low-quality cells if they met the following criteria: (1) < 1000 unique molecular identifiers (UMIs); (2) < 500 genes contained per cell; and (3) > 25% UMIs derived from the mitochondrial genome. A total of 100,201 nuclei were obtained with a median of 3451 UMIs and 1,681 genes from the 12 samples. Highly variable genes used for downstream dimensionality reduction analysis were determined using the FindVariableFeatures function of Seurat, with a default parameter of 2000 features. The top 20 Principal Components (PCs) from PC analysis were used to perform UMAP (Uniform Manifold Approximation and Projection) analysis. Unsupervised cluster analysis was conducted using the FindNeighbors and FindClusters functions at a resolution of 0.8. Finally, a total of 31 clusters were visualized in a two-dimensional space.

Cell-type annotation and neuronal subclustering

The FindAllMarkers function in Seurat was employed to determine unique enriched differentially expressed genes (DEGs) (log2 fold change >0.26 with Wilcoxon test and adjusted *p* value < 0.01) in a cluster relative to others. These cell clusters were first identified by using the expression pattern of a set of canonical cell type-specific markers and those identified neurons were reclustered into 17 subclusters at a resolution of 0.1. Neuronal subtypes were identified by the expression pattern of marker genes related to the synthesis and transportation of neurotransmitters according to literature[14,46,65].

DEGs identification and functional enrichment analysis

DEGs between the WT and $Arvcf^{-/-}$ mice for saline or nicotine-treated dopaminergic neurons were identified using a Wilcoxon rank sum test with a *p*-adj-value < 0.05, calculated using the False Discovery Rate (FDR) correction. Moreover, the absolute value of log2(fold change) >0.26 and the positive rate of DEGs in both groups of cells is greater than 10%. All significant DEGs after correction were used for the functional enrichment analysis. The functional enrichment analysis of the DEGs was conducted using Gene Ontology (http://geneontology.org). The ridge plot depicting the expression levels of dopamine biosynthesis pathway-related genes in dopaminergic neurons across different groups was generated using the RidgePlot() function from the Seurat package.

RNAscope in situ hybridization

Mice were anesthetized with sodium pentobarbital (50 mg /kg, *i.p.* injection) and infused with 150 mL cold saline and 50 mL 4% paraformaldehyde through the left ventricle of the heart. After decapitation, the intact mouse brain tissues were carefully dissected out and post-fixed in 4% paraformaldehyde at 4 °C for 24 h. Brains were then dehydrated in a 30% sucrose solution at 4 °C for 72 h. Frozen mouse brains were coronally sectioned into 10-μm-thick slices and each section was mounted at the center of SuperFrost Plus Slides (Thermo Fisher Scientific, 12-550-15). Prepared brain slices were stored at −80 °C for further experiments, performed within 1 week.

RNAscope was then performed using the RNAScope® Multiplex Fluorescent V2 Assay (ACD Bio, USA) and the HybEZ™ II Hybridization System (ACD Bio, USA) according to the manufacturer's instructions. All the agents, equipment, and *Arvcf* mRNA probes were purchased from ACD. Prepared slides were baked at 60 °C for 30 min. Slices were fixed for 15 min in chilled 4% paraformaldehyde in PBS and then rinsed in PBS and dehydrated in an ascending ethanol series (50%, 70%, 100% ×2 for 5 min each). After 5 min of air-drying at room temperature (RT), tissues were incubated with RNAscope hydrogen peroxide for 10 min to block endogenous peroxidases and were then washed twice with distilled water. The HybEZ™ II hybridization furnace was preheated to 40 °C for at least 1 h. After rewarming for 30 min at RT, the slices were fixed with fresh cold 4% PFA for 30 min. The slices were then washed and treated with 2 drops of protease III for 30 min at 40 °C. Probe hybridization was performed by incubating brain slices with 2 drops of designed probes (RNAscope Probe Mm-*Arvcf*-C1) for 2 h in a HybEZ™ hybridization furnace. Positive and negative controls (RNAscope 3-plex Positive-control Probe-Mm and RNAscope 3-plex Negative-control Probe) were performed in parallel. For signal amplification, slices were sequentially incubated with 2 drops of AMP1, AMP2, and AMP3 for 30 min. Hybridized signals were tagged with fluorescent dyes Opal 570 (Akoya Biosciences, USA). Finally, the slides were counterstained with DAPI for 30 s at RT.

The staining slices were imaged at 20× objective on a confocal microscope system (Olympus, VS120, Japan) and the images were analyzed using ImageJ software. VSI format image files were imported and opened by plugins in ImageJ software and then the corresponding scale was set. For cell counting statistics, we manually marked the nuclei of target cells in the region of interest and the ImageJ software will automatically count the number of marked cells. Similarly, ImageJ was used to measure the average fluorescence intensity of single-channel *Arvcf*'s mRNA. The ROI Manager of ImageJ was employed to outline regions of the same area within the VTA of each sample and then the average fluorescence intensity of these areas were measured. The specific operation method referred to the literature on the analysis methods of ImageJ in immunofluorescence staining images[66].

Histological verifications and immunohistochemistry

The preparation of brain slices was the same as described above for the RNAscope assay. Slices (50 μm) for verifying virus expression and optic

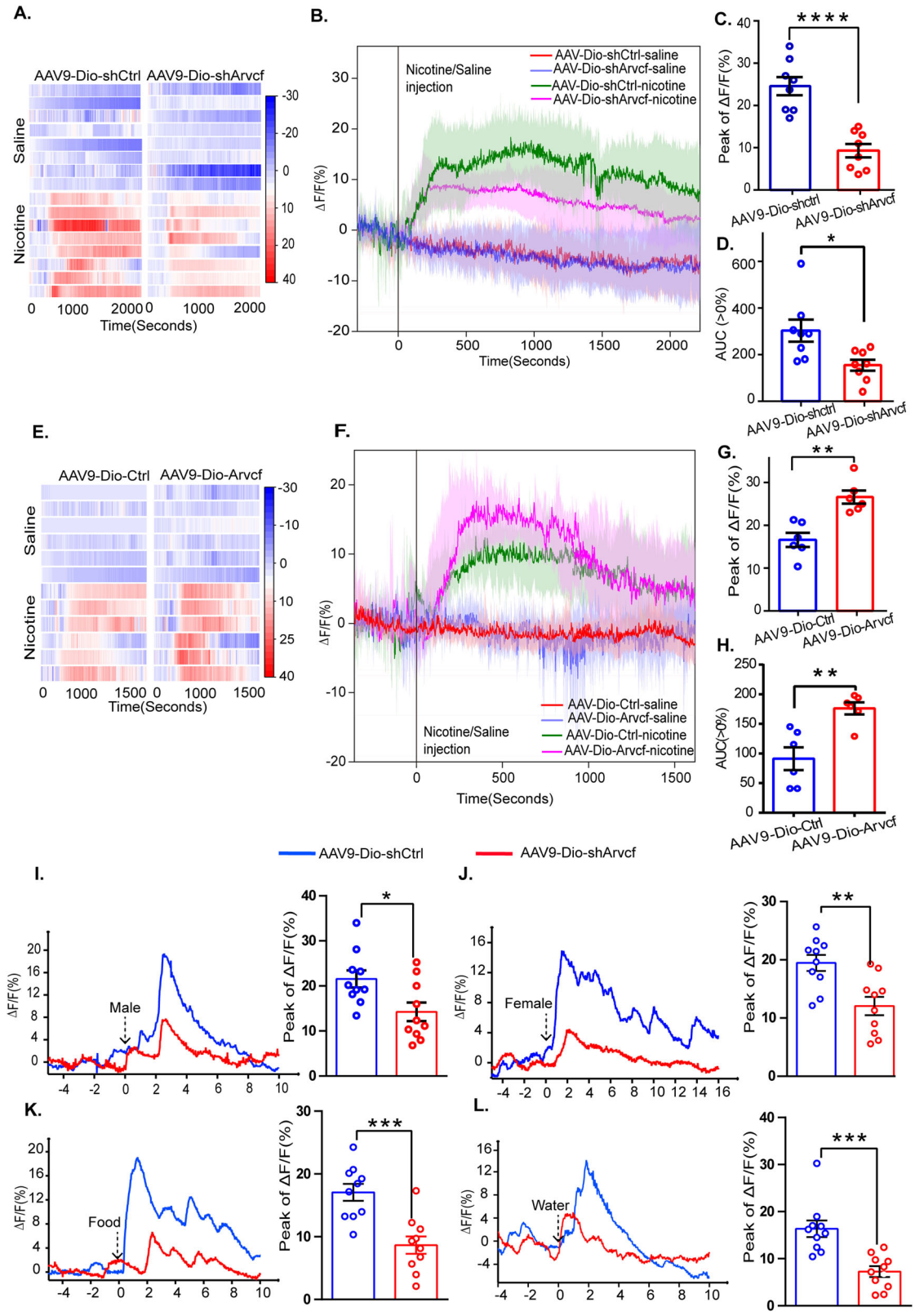

fiber locations were co-stained with DAPI (1:1000, Invitrogen) for 30 s. For tyrosine hydroxylase (TH) staining, after three washes in PBS for 5 min each, slices (30 μm) were permeabilized with 0.25% Triton-X 100 for 20 min. Next, the slices (30 μm) were incubated in blocking buffer containing 5% goat serum and 3% BSA for 2 h at RT and stained in rabbit anti-TH antibody (1:200, Proteintech) at 4 °C overnight. On the following day, slices were rewarmed for 30 min and washed in PBS containing 0.1% Tween-20 (0.1% PBST) three times for 10 min each.

Slices were then incubated for 2 h in secondary antibodies (Alexa Fluor 647 goat anti-rabbit IgG, 1:500, Abcam; FITC goat anti-rabbit IgG, 1:200, Proteintech). Following four washes with 0.1% PBST, the slices were incubated with DAPI for 1 min and imaged at 20× objective on a confocal

Fig. 5 | Specifically altering *Arvcf* expression in dopaminergic neurons affects dopamine transmission in the VTA-NAc circuit induced by nicotine reward and natural reward stimuli. A, **B** Changes of NAc dopamine release signals in NAc after knockdown *Arvcf* in VTA dopaminergic neurons of TH-cre mice under nicotine or saline stimulus. Heatmap (**A**) and average (**B**, mean ± 95% CI; vertical line, start of nicotine or saline injection) dopamine transients of neurons in NAc of AAV-Dio-sh*Arvcf* mice ($n = 8$) and corresponding control mice ($n = 8$). Statistics of peak value (**C**) and AUC (**D**) of the transients of dopamine signal in AAV-Dio-sh*Arvcf* mice and corresponding control mice under nicotine stimulus. **E**, **F** Changes of NAc dopamine release signals after overexpressing *Arvcf* in VTA dopaminergic neurons of TH-cre mice under nicotine or saline stimulus. Heatmap (**E**) and average (**F**; mean ± 95% CI; vertical line, start of nicotine or saline injection) dopamine transients of neurons in NAc of AAV-Dio-*Arvcf* mice ($n = 6$) and corresponding control mice ($n = 6$). Statistics of peak value (**G**) and AUC (**H**) of the transients of dopamine signal in AAV-Dio-*Arvcf* mice and corresponding control mice under nicotine stimulus. Representative dopamine transients in NAc of AAV-Dio-sh*Arvcf* male mice and control mice under homosexual social stimuli (panel **I**) and heterosexual social stimuli (**J**). Representative dopamine transients in NAc of AAV-Dio-sh*Arvcf* mice and control mice under food intake (**K**) and water drink (**L**) stimuli (Left). The peak value statistics of the transients of dopamine signal in AAV-Dio-sh*Arvcf* mice ($n = 10$) and control mice ($n = 10$) (right). Data are shown as Mean ± S.E.M.; Two-tailed unpaired t-tests, $^{*}p < 0.05$, $^{**}p < 0.01$,$^{***}p < 0.001$, N.S. = not significant.

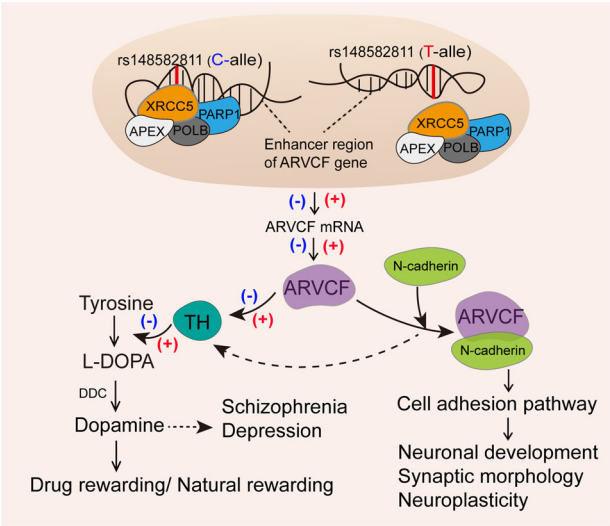

Fig. 6 | Proposed *Arvcf* working model for Xrcc5-*Arvcf*-N-cadherin signal pathway in dopamine-mediated drug addictions and mental disorders. The transcription factor XRCC5 binds to the DNA fragment containing rs148582811 and allele-specifically regulated *Arvcf* expression at the mRNA and protein levels. *Arvcf* promotes the expression of tyrosine hydroxylase (TH) leading to the increased dopamine synthesis. *Arvcf* can also regulate the development of neuronal morphologies by interacting with N-cadherin. Taken together, we conclude that *Arvcf* participates in the development of ND by regulating dopamine synthesis and neuronal development. This may also imply a potential role for *Arvcf* in more addicted phenotypes and other mental disorders such as schizophrenia and depression.

microscope system (Olympus, VS120, Japan). Finally, the images were analyzed by ImageJ and the analysis method was similar to that used in the RNAscope assay above.

High performance liquid chromatography-mass spectrometry (HPLC-MS)

Concentrations of dopamine neurotransmitters in VTA were examined by HPLC-MS technique. VTA tissues from *Arvcf*-KO mice and WT mice were obtained as described in SnRNA-seq analysis. The isolated brain tissues were weighed individually, and 15 μL of cold ultrapure water was added per mg of tissue. The tissue was homogenized for 1 min using a homogenizer and then centrifuged at 12,000 rpm in a 4 °C centrifuge for 10 min. For catecholamine neurotransmitters, 210 μL of the supernatant is taken and subjected to vacuum freeze-drying. After drying, 60 μL of cold ultrapure water was added to re-suspend the sample, which was then mixed thoroughly and prepared for analysis. For amino acid neurotransmitters, 10 μL of the supernatant was taken and mixed with 10 μL of ultrapure water and 40 μL of isopropanol solution containing 0.1% formic acid. The mixture was centrifuged at 12,000 rpm in a 4 °C centrifuge for 10 min. 10 μL of the supernatant was taken and added with 70 μL of borate buffer and 20 μL of AccQ Tag derivatization reagent (from the Kairos amino acid assay kit, USA). The mixture is then heated at 55 °C for 10 min, followed by the addition of 400 μL of cold ultrapure water, which is subsequently mixed and prepared for analysis.

The processed brain tissue supernatants were chromatographically separated by ACQUITY UPLC I-Class system (Waters Co., Milford, MA, USA). The mobile phase components consisted of solvent A, a 0.1% aqueous formic acid solution, and solvent B, pure acetonitrile. The chromatographic separation of supernatants was performed under conditions of a flow rate of 0.4 mL/min, an injection volume of 5 μL, and a column temperature of 35 °C.

The constituents were then detected by Xevo TQ-XS tandem quadrupole mass spectrometry system (Waters Co., Milford, MA, USA) with an ion source voltage of 3.0 kV and a temperature of 150 °C, a desolvation temperature of 400 °C, a desolvation gas flow rate of 800 L/h, and a conical pore gas flow rate of 150 L/h. The peak areas of the targeted data were analyzed using TargetLynx quantitative software, and the concentration was calculated using a standard curve. The quantitative results were obtained using the standard curve method.

Fiber photometry analysis of dopamine release induced by natural reward stimuli

We first detected signal changes in dopamine release in response to social stimulus in mice. After recording a stable baseline for the test mouse over 5 min, a male mouse of similar age to the test male mouse was introduced into the home cage of the test male mouse, and the dopamine release signals during 10 min of free social interaction were recorded. Subsequently, the male mouse was tested following the same procedure for detecting dopamine signals under social stimulation with an age-matched female mouse. During free social interactions, we identified investigation behavior of the test mice. "Investigation" was defined as close contact with any part of the intruder's body[52]. The dopamine signals at the initial investigation were used for statistical analysis.

For food and water stimulus, mice were subjected to a 24-h fast from food and water. Following a 5 min baseline recording, food was provided in the home cage of the test mouse and the behavior and dopamine signals of the mouse while eating were recorded for 10 min. Subsequently, mice were tested using the same procedure for detecting dopamine signals under water stimulation. The signals of the test mice during initial water consumption or feeding were used for statistical analysis.

For natural reward stimuli, the operation of the optical fiber recording is consistent with the above detection of nicotine-induced dopamine release and the first 10 s of natural stimulation was used as a baseline for$\Delta F/F0$ calculation.

Statistical analysis

All experimental data were analyzed using GraphPad Prism 6 or Origin and are shown as Mean ± Standard Error (SEM). We used two-tailed unpaired *t*-test to compare the two groups and two-way ANOVA with Bonferroni's correction to compare groups more than 3 with two factors. $P < 0.05$ was considered statistically significant. A detailed description of sample size, statistical methods and values is given in Supplementary Data 5 for all experimental results reported in this paper. The raw data used for statistical plotting have been provided in Supplementary Data 6.

Reporting summary

Further information on research design is available in the Nature Portfolio Reporting Summary linked to this article.

Data availability

The sequencing data has been deposited in the Genome Sequence Archive (GSA) database with access number of CRA016632 (https://ngdc.cncb.ac.cn/gsub/). Additional information for this study is available from the corresponding author at ml2km@zju.edu.cn.

Received: 23 August 2024; Accepted: 26 February 2025;
Published online: 13 March 2025

References

1. Benowitz, N. L. Nicotine addiction. *N. Engl. J. Med.* **362**, 2295–2303 (2010).
2. Wills, L. et al. Neurobiological mechanisms of nicotine reward and aversion. *Pharmacol. Rev.* **74**, 271–310 (2022).
3. Robinson, T. E. & Berridge, K. C. The incentive-sensitization theory of addiction 30 years on. *Annu. Rev. Psychol.* https://doi.org/10.1146/annurev-psych-011624-024031 (2024).
4. Pascoli, V., Terrier, J., Hiver, A. & Luscher, C. Sufficiency of mesolimbic dopamine neuron stimulation for the progression to addiction. *Neuron* **88**, 1054–1066 (2015).
5. Nestler, E. J. Is there a common molecular pathway for addiction? *Nat. Neurosci.* **8**, 1445–1449 (2005).
6. Yuan, L. & Arikkath, J. Functional roles of p120ctn family of proteins in central neurons. *Semin. Cell Dev. Biol.* **69**, 70–82 (2017).
7. Donta, M. S. et al. p120-catenin subfamily members have distinct as well as shared effects on dendrite morphology during neuron development in vitro. *Front. Cell Neurosci.* **17**, 1151249 (2023).
8. Mendez-Vazquez, H. et al. The autism-associated loss of delta-catenin functions disrupts social behavior. *Proc. Natl. Acad. Sci. USA* **120**, e2300773120 (2023).
9. Xu, M. et al. Melatonin ameliorates sleep-wake disturbances and autism-like behaviors in the Ctnnd2 knock out mouse model of autism spectrum disorders. *Genes Brain Behav.* **22**, e12852 (2023).
10. Adegbola, A. et al. Disruption of CTNND2, encoding delta-catenin, causes a penetrant attention deficit disorder and myopia. *HGG Adv.* **1**, https://doi.org/10.1016/j.xhgg.2020.100007 (2020).
11. Yang, Z. et al. Single nucleotide polymorphisms rs148582811 regulates its host gene ARVCF expression to affect nicotine-associated hippocampus-dependent memory. *iScience* **26**, 108335 (2023).
12. Li, M. D. et al. Integrative analysis of genetics, epigenetics and RNA expression data reveal three susceptibility loci for smoking behavior in Chinese Han population. *Mol. Psychiatry* https://doi.org/10.1038/s41380-024-02599-1 (2024).
13. Shi, X., Wang, Y., Yang, Z., Yuan, W. & Li, M. D. Identification and validation of a novel gene ARVCF associated with alcohol dependence among Chinese population. *iScience* **27**, 110976 (2024).
14. Phillips, R. A. et al. An atlas of transcriptionally defined cell populations in the rat ventral tegmental area. *Cell Rep.* **39**, 110616 (2022).
15. Hou, G., Hao, M., Duan, J. & Han, M. H. The formation and function of the VTA dopamine system. *Int. J. Mol. Sci.* **25**, https://doi.org/10.3390/ijms25073875 (2024).
16. Morales, M. & Margolis, E. B. Ventral tegmental area: cellular heterogeneity, connectivity and behaviour. *Nat. Rev. Neurosci.* **18**, 73–85 (2017).
17. Gahring, L. C., Persiyanov, K. & Rogers, S. W. Neuronal and astrocyte expression of nicotinic receptor subunit beta4 in the adult mouse brain. *J. Comp. Neurol.* **468**, 322–333 (2004).
18. Zoli, M., Pucci, S., Vilella, A. & Gotti, C. Neuronal and extraneuronal nicotinic acetylcholine receptors. *Curr. Neuropharmacol.* **16**, 338–349 (2018).
19. Dou, Y. N. et al. Single-neuron projectome-guided analysis reveals the neural circuit mechanism underlying endogenous opioid antinociception. *Natl. Sci. Rev.* **11**, nwae195 (2024).
20. Du, Y. et al. The contributions of Mu-opioid receptors on glutamatergic and GABAergic neurons to analgesia induced by various stress intensities. *eNeuro* **9**, https://doi.org/10.1523/ENEURO.0487-21.2022 (2022).
21. Chaudun, F. et al. Distinct micro-opioid ensembles trigger positive and negative fentanyl reinforcement. *Nature* **630**, 141–148 (2024).
22. Murlanova, K. et al. Loss of astrocytic micro opioid receptors exacerbates aversion associated with morphine withdrawal in mice: role of mitochondrial respiration. *Cells* **12**, https://doi.org/10.3390/cells12101412 (2023).
23. Jimenez-Blasco, D. et al. Glucose metabolism links astroglial mitochondria to cannabinoid effects. *Nature* **583**, 603–608 (2020).
24. Navarrete, M. & Araque, A. Endocannabinoids mediate neuron-astrocyte communication. *Neuron* **57**, 883–893 (2008).
25. Lu, H. C. & Mackie, K. An Introduction to the Endogenous Cannabinoid System. *Biol Psychiatry* **79**, 516–525 (2016).
26. Maskos, U. et al. Nicotine reinforcement and cognition restored by targeted expression of nicotinic receptors. *Nature* **436**, 103–107 (2005).
27. Drenan, R. M. et al. In vivo activation of midbrain dopamine neurons via sensitized, high-affinity alpha 6 nicotinic acetylcholine receptors. *Neuron* **60**, 123–136 (2008).
28. Steidl, S., Wasserman, D. I., Blaha, C. D. & Yeomans, J. S. Opioid-induced rewards, locomotion, and dopamine activation: A proposed model for control by mesopontine and rostromedial tegmental neurons. *Neurosci Biobehav Rev* **83**, 72–82 (2017).
29. Zell, V. et al. VTA Glutamate Neuron Activity Drives Positive Reinforcement Absent Dopamine Co-release. *Neuron* **107**, 864–873.e864 (2020).
30. Dedic, N. et al. Chronic CRH depletion from GABAergic, long-range projection neurons in the extended amygdala reduces dopamine release and increases anxiety. *Nat Neurosci* **21**, 803–807 (2018).
31. Du, Y. et al. Dopamine release and negative valence gated by inhibitory neurons in the laterodorsal tegmental nucleus. *Neuron* **111**, 3102–3118.e3107 (2023).
32. Corkrum, M. & Araque, A. Astrocyte-neuron signaling in the mesolimbic dopamine system: the hidden stars of dopamine signaling. *Neuropsychopharmacology* **46**, 1864–1872 (2021).
33. Huebner, R. J. et al. ARVCF catenin controls force production during vertebrate convergent extension. *Dev Cell* **57**, 1119–1131.e1115 (2022).
34. Castane, A., Soria, G., Ledent, C., Maldonado, R. & Valverde, O. Attenuation of nicotine-induced rewarding effects in A2A knockout mice. *Neuropharmacology* **51**, 631–640 (2006).
35. De Biasi, M. & Dani, J. A. Reward, addiction, withdrawal to nicotine. *Annu Rev Neurosci* **34**, 105–130 (2011).
36. Volkow, N. D. & Blanco, C. Substance use disorders: a comprehensive update of classification, epidemiology, neurobiology, clinical aspects, treatment and prevention. *World Psychiatry* **22**, 203–229 (2023).
37. Volkow, N. D., Wise, R. A. & Baler, R. The dopamine motive system: implications for drug and food addiction. *Nat Rev Neurosci* **18**, 741–752 (2017).
38. Subramaniyan, M. & Dani, J. A. Dopaminergic and cholinergic learning mechanisms in nicotine addiction. *Ann N. Y Acad Sci* **1349**, 46–63 (2015).
39. Speranza, L., di Porzio, U., Viggiano, D., de Donato, A. & Volpicelli, F. Dopamine: The Neuromodulator of Long-Term Synaptic Plasticity, Reward and Movement Control. *Cells* **10**, https://doi.org/10.3390/cells10040735 (2021).
40. Ikemoto, S. & Panksepp, J. The role of nucleus accumbens dopamine in motivated behavior: a unifying interpretation with special reference to reward-seeking. *Brain Res Brain Res Rev* **31**, 6–41 (1999).
41. Parker, N. F. et al. Reward and choice encoding in terminals of midbrain dopamine neurons depends on striatal target. *Nat Neurosci* **19**, 845–854 (2016).

42. Roitman, M. F., Wheeler, R. A. & Carelli, R. M. Nucleus accumbens neurons are innately tuned for rewarding and aversive taste stimuli, encode their predictors, and are linked to motor output. *Neuron* **45**, 587–597 (2005).
43. Liu, H. M. et al. IPAC integrates rewarding and environmental memory during the acquisition of morphine CPP. *Sci Adv* **9**, eadg5849 (2023).
44. Daza-Losada, M. et al. Rewarding effects and reinstatement of MDMA-induced CPP in adolescent mice. *Neuropsychopharmacology* **32**, 1750–1759 (2007).
45. Sun, F. et al. A Genetically Encoded Fluorescent Sensor Enables Rapid and Specific Detection of Dopamine in Flies, Fish, and Mice. *Cell* **174**, 481–496.e419 (2018).
46. Willmore, L, et al. Overlapping representations of food and social stimuli in mouse VTA dopamine neurons. Neuron https://doi.org/10.1016/j.neuron.2023.08.003 (2023).
47. Tasic, B. et al. Adult mouse cortical cell taxonomy revealed by single cell transcriptomics. *Nat Neurosci* **19**, 335–346 (2016).
48. Hatsukami, D. K., Stead, L. F. & Gupta, P. C. Tobacco addiction. *Lancet* **371**, 2027–2038 (2008).
49. Le Foll, B. et al. Tobacco and nicotine use. *Nat Rev Dis Primers* **8**, 19 (2022).
50. Spanagel, R. Animal models of addiction. *Dialogues Clin Neurosci* **19**, 247–258 (2017).
51. O'Dell, L. E. & Khroyan, T. V. Rodent models of nicotine reward: what do they tell us about tobacco abuse in humans? *Pharmacol Biochem Behav* **91**, 481–488 (2009).
52. Dai, B. et al. Responses and functions of dopamine in nucleus accumbens core during social behaviors. *Cell Rep*. **40**, 111246 (2022).
53. Wang, J. et al. Basal forebrain mediates prosocial behavior via disinhibition of midbrain dopamine neurons. *Proc Natl Acad Sci USA* **118**, https://doi.org/10.1073/pnas.2019295118 (2021).
54. Cai, X., Stringer, J. M., Zerafa, N., Carroll, J. & Hutt, K. J. Xrcc5/Ku80 is required for the repair of DNA damage in fully grown meiotically arrested mammalian oocytes. *Cell Death Dis* **14**, 397 (2023).
55. Giffin, W. et al. Sequence-specific DNA binding by Ku autoantigen and its effects on transcription. *Nature* **380**, 265–268 (1996).
56. Gu, Y. et al. SNORD88B-mediated WRN nucleolar trafficking drives self-renewal in liver cancer initiating cells and hepatocarcinogenesis. *Nat Commun* **15**, 6730 (2024).
57. Gu, Z. et al. Overexpression of CLC-3 is regulated by XRCC5 and is a poor prognostic biomarker for gastric cancer. *J Hematol Oncol* **11**, 115 (2018).
58. Zhang, Z. et al. XRCC5 cooperates with p300 to promote cyclooxygenase-2 expression and tumor growth in colon cancers. *PLoS One* **12**, e0186900 (2017).
59. Halperin, D. et al. CDH2 mutation affecting N-cadherin function causes attention-deficit hyperactivity disorder in humans and mice. *Nat Commun* **12**, 6187 (2021).
60. Douma, E. H. & de Kloet, E. R. Stress-induced plasticity and functioning of ventral tegmental dopamine neurons. *Neurosci Biobehav Rev*. **108**, 48–77 (2020).
61. Xin, J., Shan, W., Li, J., Yu, H. & Zuo, Z. Activation of the Lateral Habenula-Ventral Tegmental Area Neural Circuit Contributes to Postoperative Cognitive Dysfunction in Mice. *Adv Sci (Weinh)* **9**, e2202228 (2022).
62. Morel, C. et al. Midbrain projection to the basolateral amygdala encodes anxiety-like but not depression-like behaviors. *Nat Commun* **13**, 1532 (2022).
63. Kempadoo, K. A., Mosharov, E. V., Choi, S. J., Sulzer, D. & Kandel, E. R. Dopamine release from the locus coeruleus to the dorsal hippocampus promotes spatial learning and memory. *Proc Natl Acad Sci USA* **113**, 14835–14840 (2016).
64. Xue, Y. X. et al. A memory retrieval-extinction procedure to prevent drug craving and relapse. *Science* **336**, 241–245 (2012).
65. Mickelsen, L. E. et al. Single-cell transcriptomic analysis of the lateral hypothalamic area reveals molecularly distinct populations of inhibitory and excitatory neurons. *Nat Neurosci* **22**, 642–656 (2019).
66. Jensen, E. C. Quantitative analysis of histological staining and fluorescence using ImageJ. *Anat Rec (Hoboken)* **296**, 378–381 (2013).

Acknowledgements

This study was supported in part by the National Natural Science Foundation of China (82271560), China Precision Medicine Initiative (2016YFC0906300), Research Project of Joint Research Institute of Tobacco and Health of China (No. 2021JC06), Research Center for Air Pollution and Health of Zhejiang University, the State Key Laboratory for Diagnosis and Treatment of Infectious Diseases of the First Affiliated Hospital of Zhejiang University, and Nanhu Brain-computer Interface Institute (010904013).

Author contributions

Y.W., Z.Y., X.S., H.H., W.Y., Y.S., and B.Z. conducted the experiments; Y.W., X.S., and H.H. participated in data analysis; Z.Y., W.Y., X.M.L., H.L., and M.D.L. provided the resources and managed the project; Y.W., Z.Y., A.N.L., X.M.L., H.L., and M.D.L. participated in article writing and editing; M.D.L. conceived the study and was involved in every step of the study. All authors approved the article as submitted.

Competing interests

The authors declare no competing interests.

Additional information

Supplementary information The online version contains supplementary material available at https://doi.org/10.1038/s42003-025-07837-y.

Correspondence and requests for materials should be addressed to Hong Lian or Ming D. Li.

Peer review information *Communications Biology* thanks Brandon Henderson and the other, anonymous, reviewer(s) for their contribution to the peer review of this work. Primary Handling Editors: Fereshteh Nugent and Benjamin Bessieres.